Chemistry & Biology
Article

Structural and Mechanistic Studies on γ-Butyrobetaine Hydroxylase

Ivanhoe K.H. Leung,[1,4] Tobias J. Krojer,[2,4] Grazyna T. Kochan,[2,4] Luc Henry,[1,4] Frank von Delft,[2,3] Timothy D.W. Claridge,[1] Udo Oppermann,[2,3] Michael A. McDonough,[1,*] and Christopher J. Schofield[1,*]
[1]The Department of Chemistry and the Oxford Centre for Integrative Systems Biology, Chemistry Research Laboratory, University of Oxford, 12 Mansfield Road, Oxford OX1 3TA, UK
[2]Structural Genomics Consortium, University of Oxford, Old Road Campus Roosevelt Drive, Headington OX3 7DQ, UK
[3]The Botnar Research Centre, Oxford Biomedical Research Unit, Oxford OX3 7LD, UK
[4]These authors contributed equally to this work
*Correspondence: michael.mcdonough@chem.ox.ac.uk (M.A.M.), christopher.schofield@chem.ox.ac.uk (C.J.S.)
DOI 10.1016/j.chembiol.2010.09.016

SUMMARY

The final step in carnitine biosynthesis is catalyzed by γ-butyrobetaine (γBB) hydroxylase (BBOX), an iron/2-oxoglutarate (2OG) dependent oxygenase. BBOX is inhibited by trimethylhydrazine-propionate (THP), a clinically used compound. We report structural and mechanistic studies on BBOX and its reaction with THP. Crystallographic and sequence analyses reveal that BBOX and trimethyllysine hydroxylase form a subfamily of 2OG oxygenases that dimerize using an N-terminal domain. The crystal structure reveals the active site is enclosed and how THP competes with γBB. THP is a substrate giving formaldehyde (supporting structural links with histone demethylases), dimethylamine, malonic acid semi-aldehyde, and an unexpected product with an additional carbon-carbon bond resulting from N-demethylation coupled to oxidative rearrangement, likely via an unusual radical mechanism. The results provide a basis for development of improved BBOX inhibitors and may inspire the discovery of additional rearrangement reactions.

INTRODUCTION

In animals, many plants and microorganisms carnitine (L-3-hydroxy-4-*N,N,N*-trimethylaminobutyrate, CAR) plays an essential metabolic role by enabling transport of long-chain fatty acids into the mitochondria. CAR is also involved in transport of the products of β oxidation, fatty acid storage, excretion of toxic products, and maintaining acyl-coenzyme-A/coenzyme-A homeostasis (Vaz and Wanders, 2002). In animals CAR is obtained from the diet and by endogenous biosynthesis. CAR is used as food supplement to promote fatty acid metabolism and is produced either in racemic form by synthesis or in chiral form by fermentation (Naidu et al., 2000; Brass et al., 1994).

In animals CAR biosynthesis occurs from N^{ε}-trimethyllysine, which is produced by hydrolysis of methylated proteins (Figure 1A). Pioneering work demonstrated that two CAR biosynthesis steps are catalyzed by Fe(II) and 2-oxoglutarate (2OG) dependent oxygenases, N^{ε}-trimethyllysine hydroxylase (TMLH) and γ-butyrobetaine (γBB) hydroxylase (BBOX). (Hulse et al., 1978; Lindstedt, 1967, 1977; Englard et al., 1985). BBOX is the target for 3-(2,2,2-trimethylhydrazine)propionate (THP), which is used to treat myocardial infarction (Simkhovich et al., 1988; Dambrova et al., 2002). THP is proposed to lower the levels of reactive oxidizing species associated with fatty acid metabolism by preventing CAR-mediated transport.

We report structural and mechanistic analyses on human BBOX and its inhibition by THP. The results reveal a close relationship between BBOX and TMLH and link the CAR biosynthesis enzymes with the 2OG-dependent histone N^{ε}-methyl lysine demethylases. Studies with γBB analogs and on the mechanism of action of THP reveal that BBOX can catalyze N-methyl demethylation and that the reaction of THP with BBOX involves an unprecedented rearrangement involving N-methyl cleavage and a novel C-*C* bonding forming reaction.

RESULTS

Characterization of BBOX Activity

To investigate its relationship with other human 2OG oxygenases and the mechanism of action of THP, we produced recombinant human BBOX and developed an NMR assay (Figure 1B). The results reveal human BBOX to be highly active and dependent on Fe(II) (see Figure S1A and Table S1A, entry I, available online) and show CAR production to be tightly coupled to 2OG oxidation. BBOX activity was stimulated by potassium ions and reducing agents, including but not limited to ascorbate, and subject to substrate inhibition (Figure S1A), as observed with prokaryotic and partially purified animal BBOX (Lindstedt et al., 1977; Wehbie et al., 1988). The observations with reducing agents are consistent with mouse model work using animals that cannot produce ascorbate (Furusawa et al., 2008).

Overall Structure

We crystallized BBOX employing Zn(II) as an Fe(II) substitute and *N*-oxalylglycine (NOG, an unreactive 2OG analog) (Table S1B, entry I) and γBB. The resultant BBOX.Zn.NOG.γBB structure (resolution 1.82 Å) reveals a homodimer as observed in solution analyses (Galland et al., 1998; Krissinel and Henrick, 2007) (Figure 2). Each monomer comprises N- and C-terminal domains

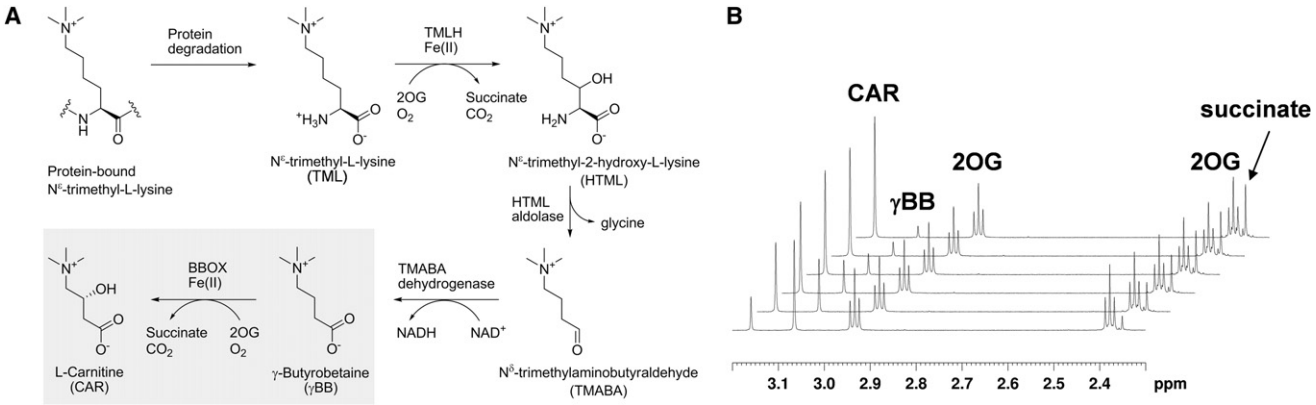

Figure 1. The Role of BBOX in CAR Biosynthesis

(A) The carnitine biosynthesis pathway.

(B) NMR monitoring of BBOX activity in real time: signals for L-Carnitine (CAR), γBB, 2OG, and succinate. Spectra are at 10-min intervals, and the first spectrum is recorded 5 min after sample mixing.

See also Figure S1 for more BBOX characterization.

linked by α-helix α3 (residue range 97–110), positioned close to the C-terminal helix (α10). The N-terminal domain (comprised of secondary elements α1, α2, β1–8) enables dimerization. Whereas dimerization via C-terminal structural elements has been observed for other 2OG oxygenases, BBOX represents the first example of dimerization via an N-terminal domain. Sequence analyses imply that TMLH similarly dimerizes via its N-terminal domain (Figure S2i). The presence of a zinc-binding site in the N-terminal domain was unexpected and is formed by a 3Cys-1His zinc-binding motif (Cys38, Cys40, Cys43, and His82). The C-terminal domain has a double-stranded β-helical core fold (DSBH, β^{I}–β^{VIII}) (Figure 2) forming the major ($\beta11^{I}$, $\beta22^{VIII}$, $\beta13^{III}$, $\beta20^{VI}$, β10, β9) and minor ($\beta12^{II}$, $\beta21^{VII}$, $\beta14^{IV}$, $\beta19^{V}$) β sheets, characteristic of 2OG oxygenases (Clifton et al., 2006). A 94 residue "insert" between DSBH strands $\beta14^{IV}$ and $\beta19^{V}$ contains three α helices (α7, α8, α9), four β strands (β15, β16, β17, β18), and one 3_{10} helix ($3_{10}4$). This insert folds over the more open end of the DSBH, forming both part of the active site and part of the dimerization interface with the N-terminal domain of the other chain in the dimer. A loop and a 3_{10}-helix ($3_{10}3$) links DSBH strand $\beta11^{I}$ with strand $\beta12^{II}$. This region (residues 184–198) also folds over the active site and is involved in substrate binding (Figure 2B); in addition, it interacts with another region comprised of the antiparallel β strands β4-β5 and helix $3_{10}2$ (residues 43–54), which extends from the N-terminal domain zinc-binding site of the other chain in the dimer. Sequence comparison of BBOX with TMLH (26% identity) implies that both the folds and active sites of the two enzymes are similar.

N-Terminal Zinc-Binding Domain

The N-terminal domain fold of BBOX is most related to that of a protein of unknown function from *Acidithiobacillus ferrooxidans* ATCC 23270 (PDB ID 3LUU; PFAM family DUF971, PF06155; DALI Z score = 10.8; rmsd 2.1 Å over 81 residues), which has many homologs (including in prokaryotes), though none other than BBOX or TMLH appear to be 2OG oxygenases. The 3Cys-1His zinc-binding motif is conserved in many of the apparent homologs (Figure S2ii). Although the equivalent N-terminal domain zinc-binding residues in the *Acidithiobacillus* protein structure appear partially disordered, it does have zinc bound, albeit using residues from different secondary structural elements (His36, Glu40, and the C-terminal carboxylate of Glu100). Cys-40 of BBOX is substituted with serine in TMLH, potentially altering metal-binding specificity in TMLH (Figures S2i and S2ii).

Active Site

The active site is enclosed by loops between $\beta11^{I}$–$\beta12^{II}$, β18–$3_{10}4$, and β strand β15 (Figure 3). The opening of a tunnel leading toward the active site, which may enable binding of oxygen and release of CO_2, is "bridged" by the side chains of Val-192 (located between $\beta11^{I}$–$\beta12^{II}$) and Ala-294 (located between β18–$3_{10}4$) (Figure 3C). The small size of the tunnel opening suggests that conformational changes by loop movements may occur to enable substrate binding and product release.

As for other 2OG oxygenases (Clifton et al., 2006), the active site metal is bound by three ligands (His-202, Asp-204, and His-347) (Figure 3). NOG binds to the metal in a bidentate manner with its 1-carboxylate coordinating via a single oxygen (*trans* to His-347) and its C-2 carbonyl oxygen (*trans* to Asp-204). The C-5 carboxylate of NOG interacts with a basic residue (Arg-360) and a hydroxyl group (Ser-229), as observed in other 2OG oxygenases; untypically a second arginine (Arg-349) is also involved in binding of the 2OG C-5 carboxylate. A water completes the octahedral coordination sphere and is positioned to form a hydrogen bond with Gln-215 Oε (2.7 Å) and the Asp-204 carboxylate (2.8 Å), suggesting that both of these residues play a role in O_2 binding. The remainder of the residues around the putative O_2-binding site are hydrophobic (Trp-181, Leu-217, Leu-362). The metal coordination site closest to C-3 of the substrate is occupied by the 2OG C-1 carboxylate. Although it is uncertain whether the crystal structure reflects the solution situation, this arrangement suggests that O_2 may bind at the position occupied by the water, necessitating a rearrangement

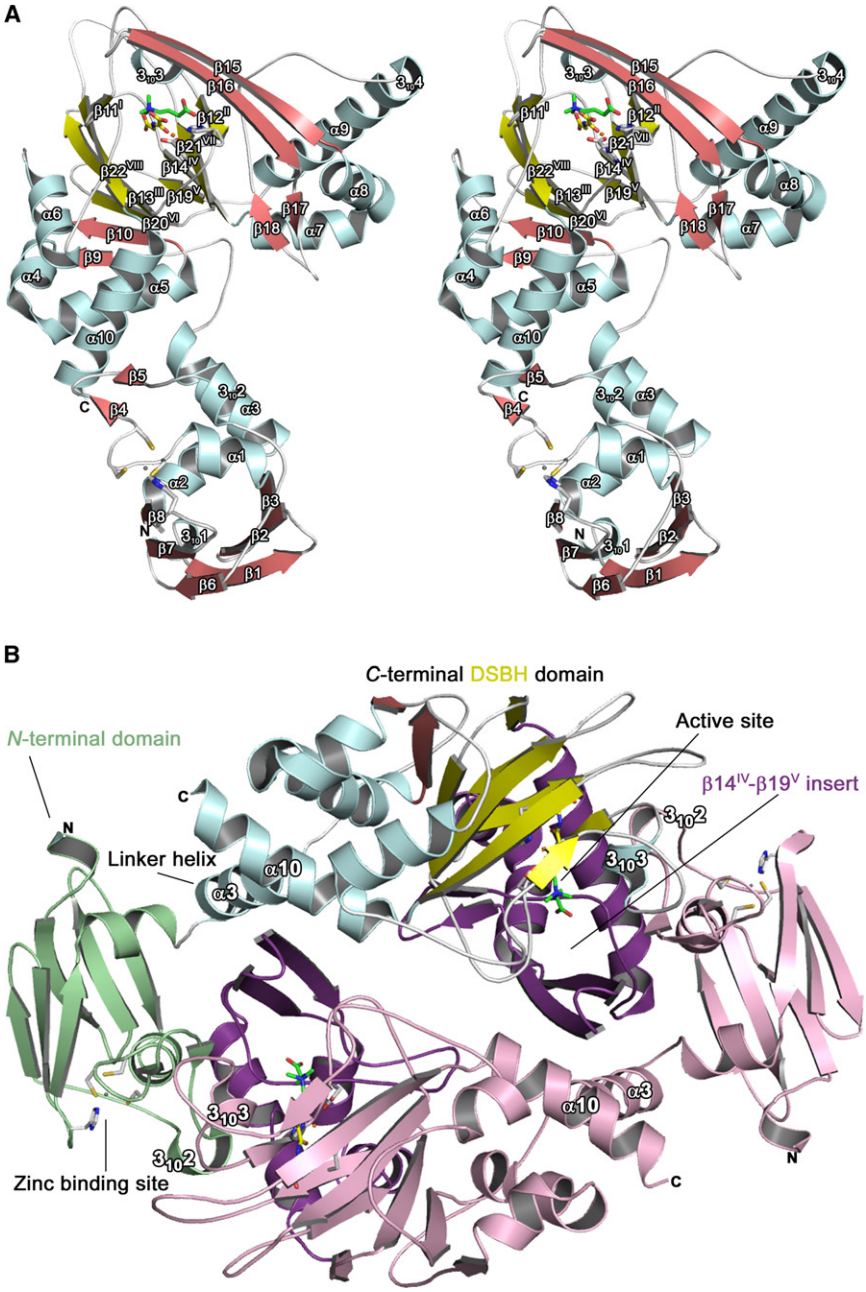

Figure 2. The Overall Fold of BBOX

(A) Stereo view ribbons representation of the BBOX:Zn:NOG:γBB structure. Colored and labeled by secondary structure elements; β strands are pink, and the core DSBH strands are highlighted in yellow, α helices are light blue, and loops are white. Metal binding residues are shown as white sticks, the Zn(II) is displayed as an orange sphere (substituting for iron at the active site) and as a gray sphere in the N-terminal domain. NOG is shown as yellow sticks and γBB as green sticks. (B) Ribbons representation of the BBOX dimer; one monomer is in pink and the other colored as in (A) except for the N-terminal Zn(II) binding domain in light green and the $\beta14^{IV}$-$\beta19^{V}$ insert, which is purple in both molecules.

See also Figure S2 for human BBOX sequence alignments.

(as proposed for other 2OG oxygenases) (Zhang et al., 2002) for the catalytically reactive ferryl intermediate (Hausinger, 2004; Hoffart et al., 2006) to be positioned adjacent to the oxidized bond. γBB binds adjacent to the metal, such that its C-3 *pro-R* C-H bond, which must undergo hydroxylation to give CAR, projects toward the metal (C-3 γBB to metal: 4.7 Å) (Englard et al., 1985) (Figure 3B).

Substrate Specificity

The γBB carboxylate is positioned to interact via hydrogen bonds with the side chains of Asn-292 (2.9 Å), Asn-191 (2.9 Å), and the backbone amide of Tyr-205 (2.9 Å) (Figures 3A and 3B). Structurally informed sequence analyses imply that BBOX and TMLH bind their substrates similarly, except that a modification ($Asn191_{BBOX}$ to $Asp131_{TMLH}$) at the observed C-1 γBB carboxylate-binding site of BBOX enables binding of the α amino group of TMLH's N^{ε}-trimethyllysine substrate (Figures S2i and S2iii).

The positively charged γBB N-trimethyl ammonium group is located in an electron-rich aromatic "cage" formed by the side chains of Tyr177, Tyr-194, and Trp-181 (Figures 3B; Figure S3i) with the side chains of two other aromatic residues positioned nearby (Tyr-205 and Tyr-366). Tyr-366 is also positioned to hydrogen bond to the side chain of Asp-204, suggesting that it may be involved in coordinating γBB binding and reactions at the metal center. The mode of binding of the N-trimethyl group is strikingly similar to the manner in which the same group binds to plant homeobox domain and Tudor domains that bind to modified histones (Huang et al., 2006; Horton et al., 2010) (Figure S3i). N-trimethyl binding also occurs with the 2OG-dependent histone N^{ε}-lysyl demethylases; however, with these enzymes the N-trimethyl binding site is less hydrophobic because one of the substrate methyl groups must be adjacent to the iron to enable demethylation (Ng et al., 2007).

Structural Insights into Specificity and Enzymatic Mechanism

Support for the crystallographically observed substrate binding mode was obtained from substrate analog studies. The carboxylate functionality is an absolute requirement for substrate binding and activity (data not shown), but the requirement for the trimethylamino group is less stringent. γBB analogs with deletion or addition of a methylene group were substrates for

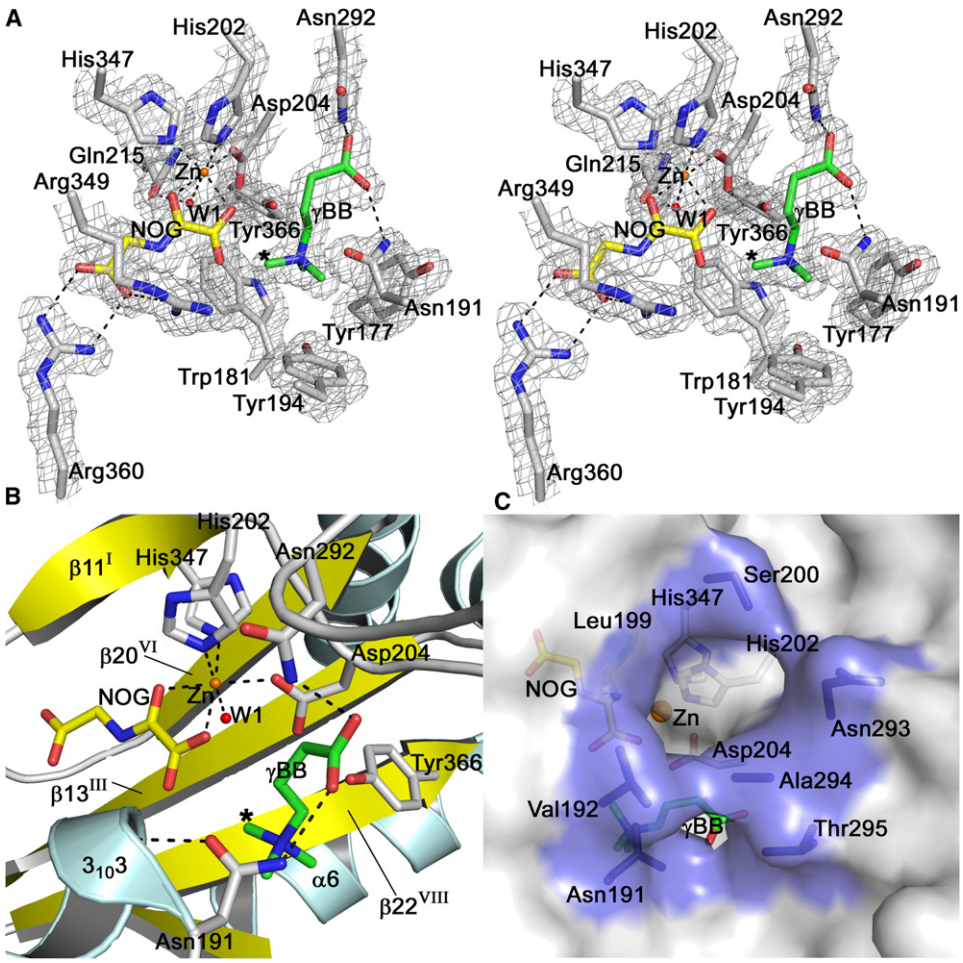

Figure 3. BBOX Active Site

(A) Stereo view representation of the electron density (2Fo-Fc electron density map shown as gray mesh contoured to 1σ) from the 1.82 Å resolution BBOX:γBB structure data. The metal is shown as an orange sphere that is coordinated by three BBOX residues (shown as white sticks), a water (red sphere), and *N*-oxalylglycine (yellow sticks). γBB is shown as green sticks. Black dashes indicate metal coordination and selected hydrogen bonds.

(B) View of the active site of BBOX in complex with Zn(II) (orange sphere), *N*-oxalylglycine (yellow sticks), and γBB (green sticks). Interactions between the γBB carboxylate and Asn-191, Asn-292 and metal coordination interactions are indicated by black dashes. Asn-191 also plays a role in capping the 3_{10} helix ($3_{10}3$) indicated by a dashed line to the backbone amide of Ala-193.

(C) Solvent accessible surface of BBOX (gray and blue) showing the opening of the tunnel bridged by residues Val-192 and Ala-294. The tunnel leads to the active site and is lined by Val-192, Ala-294, Ala-293, Asn-191, Thr-295, Leu-199 (shown as blue surface and sticks).

See also Figure S3 for BBOX ligand binding and a comparison of the BBOX and histone lysine demethylase active sites.

BBOX but were oxidized less efficiently (Table S1A, entries II and III, respectively), as was the γBB analog with two N^{ε}-methyl groups (Table S1A, entry IV).

Analysis of the γBB-binding site revealed the side chain hydrogen bond donor/acceptor atom of Asn-191 is 3.8 Å from the C-3 carbon of γBB (Figure 3), suggesting that BBOX may accept substrates having a polar group at C-3 with "D" stereochemistry; therefore, we tested the D-enantiomer of CAR (D-CAR) as a substrate for BBOX. We found that D-CAR was a substrate for BBOX (Table S1A, entry V) producing *N,N,N*-trimethylaminoacetone, presumably through facile nonenzymatic decarboxylation of an intermediate β carboxyketone formed from the C-3 dihydroxylated product (Figure S4i). Interestingly, we also found that with extended incubation times, CAR itself was a substrate, albeit poorer than γBB or D-CAR, and like the latter producing *N,N,N*-trimethylaminoacetone (Table S1A, entry VI). From a biological perspective these observations are of interest because trimethylaminoacetone has been described as a metabolite of racemic carnitine or D-CAR (Holme et al., 1982). These results rationalize a previous study whereby increased 2OG turnover was observed when D-, L-, or racemic carnitine was reacted with partially purified BBOX from human kidney and *pseudomonas* sp. AK1 (Bremer, 1983). Thus, metabolic production of *N,N,N*-trimethylaminoacetone could be minimized by using pure L-carnitine (CAR), rather than racemic carnitine, as a dietary supplement.

Inhibitor Complex

To investigate its mechanism of action, we then solved a structure of THP in complex with BBOX (1.82 Å resolution). The overall

structure revealed that despite the substitution of an amino group for the C-4 methylene of γBB, THP occupies a near-identical position compared to γBB (Figure S3i). The Tyr-366 phenolic OH is positioned to interact with the secondary amino group of THP (3.6 Å). Notably, as for γBB, the THP C-3 *pro-R* hydrogen projects toward the metal, suggesting that THP may act as a competitive substrate (THP IC_{50} 34 μM) (Table S1B, entry II).

Rearrangement Mechanism

Initial NMR studies on the reaction of THP with BBOX demonstrated that the inhibitor acts as a substrate with the same cofactor requirement as γBB (Table S1A, entry VII), as suggested by previous work conducted with native rat BBOX (Spaniol et al., 2001), and indicated the generation of several products. ^{1}H and ^{13}C NMR studies led to the identification of the hydrated form of malonic acid semi-aldehyde **2** as a major product (Figure 4A). The formation of **2**, which decarboxylates to give acetaldehyde, is consistent with a mechanism involving oxidation at C-3 of THP followed by N-N fragmentation to give a hydrolytically labile imine. However, we did not observe production of 1,1,1-trimethylhydrazinium ions (or trimethylamine), as expected for a "simple" hydroxylation followed by fragmentation; instead, we observed formation of dimethylamine. 2D NMR studies led to the identification of formaldehyde (observed as a tris-(hydroxymethyl)aminomethane buffer adduct). The observation of HCHO and dimethylamine, which must be produced by N-demethylation, provides a mechanistic link between BBOX/TMLH and the histone N^{ε}-methyl lysine demethylases (Figure S3ii). The NMR analyses also indicated the production of another initially unassigned product that was not observed with γBB. The combined NMR data suggested the structure to be $HO_2CCH_2CH(NH_2)CH_2NCH_3(CH_2OH)$ **1**. To support this assignment we prepared THP ^{13}C labeled at one of its N-methyl groups. The resultant analyses confirmed the production of the previously assigned products (formaldehyde and dimethylamine, with partial incorporation of ^{13}C in the anticipated positions) and provided additional evidence for the formation of **1**, with ^{13}C being equally distributed between the N-CH_2 and the N-CH_3 carbons (Figure 4; Figure S4ii). Derivatization of the reaction mixture of labeled THP followed by LC-MS analyses led to the isolation of the derivatized product of **1**, with partial incorporation of ^{13}C in the ratios anticipated (Figures 4D–4F).

DISCUSSION

BBOX and TMLH are closely related 2OG oxygenases belonging to a distinct subfamily that is present in most eukaryotes and many prokaryotes. BBOX is a homodimer mediated by its N-terminal zinc-binding domain. The structural studies also reveal the trimethylamino group-binding site of BBOX to be related to those of histone-binding proteins. Following from pioneering work on their roles in collagen biosynthesis, animal 2OG oxygenases have more recently been shown to play roles in fatty acid metabolism, hypoxic sensing, and nucleic acid modification. In addition to the inhibition of BBOX as a method for cardioprotection, other human 2OG oxygenases are being targeted for small molecule inhibition for the treatment of diseases, including anemia and cancer. The structural information described here will be useful in order to develop potent and selective inhibitors both of BBOX and other human 2OG oxygenases.

Comparison of the structures of BBOX in complex with cofactors, metal, and substrate or inhibitor presented here with that of a recently published apo-BBOX structure provides a possible explanation as to how substrates and products may enter and leave the active site (Tars et al., 2010). The apo-BBOX structure displays disordered loops surrounding the active site, indicating that conformational flexibility of these regions in the absence of substrate or inhibitor is possible. This suggests that an induced fit mechanism may contribute to the catalytic activity of BBOX and may explain the observation of limited accessibility to the active site in the substrate inhibitor complexes.

The analog studies suggest that BBOX accepts a wide range of substrates. In fact, when compared to generic 2OG oxygenase inhibitors such as NOG and succinate (Table S1B, entries I and III), these substrate analogs act as reasonably active competitive inhibitors (Table S1B, entries IV–VII). The observation that BBOX has a less than stringent requirement for a trimethylammonium group may be useful for the design of improved BBOX inhibitors.

In microorganisms and plants, 2OG oxygenases catalyze a very wide range of oxidative reactions (Clifton et al., 2006; Hausinger, 2004). However, to date, their reactions have been limited to hydroxylations and N-demethylations via methyl group hydroxylation in animals. We define the clinically used inhibitor THP as being a competitive substrate for BBOX. THP undergoes N-demethylation and N-N fragmentation leading to a C-C bond forming rearrangement reaction. The closest parallel to the conversion of THP to **1** in established organic reactions is the Stevens rearrangement, wherein an ylide formed by deprotonation of a quaternary amine undergoes rearrangement to give a secondary amine via migration of one of the N-alkyl groups (Figure S5) (Stevens, 1928; Vanecko et al., 2006). However, in contrast to the harsh conditions of the Stevens rearrangement, the BBOX catalyzed oxidative rearrangement of THP occurs in aqueous solution at room temperature. We propose that the BBOX-catalyzed reaction of THP involves initial reaction with an iron-oxo intermediate (Krebs et al., 2007), as involved in other 2OG oxygenase reactions, to give a radical at C-3. In the case of γBB, this can undergo a rebound process to give CAR (Figure 5A). However, with THP the presence of the secondary amine enables fragmentation of the radical intermediate to give an imine and a trimethylamine radical cation (Figure 5B). In the case of THP, fragmentation of the radical must be faster than hydroxylation because we did not observe $Me_3N^{+}NH_2$. In support of the proposed role of the Aza group of THP in inducing fragmentation, the THP analog in which the trimethylamino group was replaced with *t*-butyl or isopropyl groups led to products resulting from "normal" hydroxylation, i.e., formation of *tert*-butylamine or isopropylamine (Figure 5C; Table S1A, entries VIII and IX). Following N-N cleavage, 1,2-hydrogen shift of the trimethylamine radical cation gives a methylene radical that can add into the imine to generate the rearranged C-C framework (Figure 5D). Subsequent 1,5-hydrogen abstraction on one of the N-methyl groups by the resultant amine radical (Figure 5D'), as precedented by the abstraction step in the Hofmann-Löffler-Freytag reaction (Curran et al., 1988), followed by

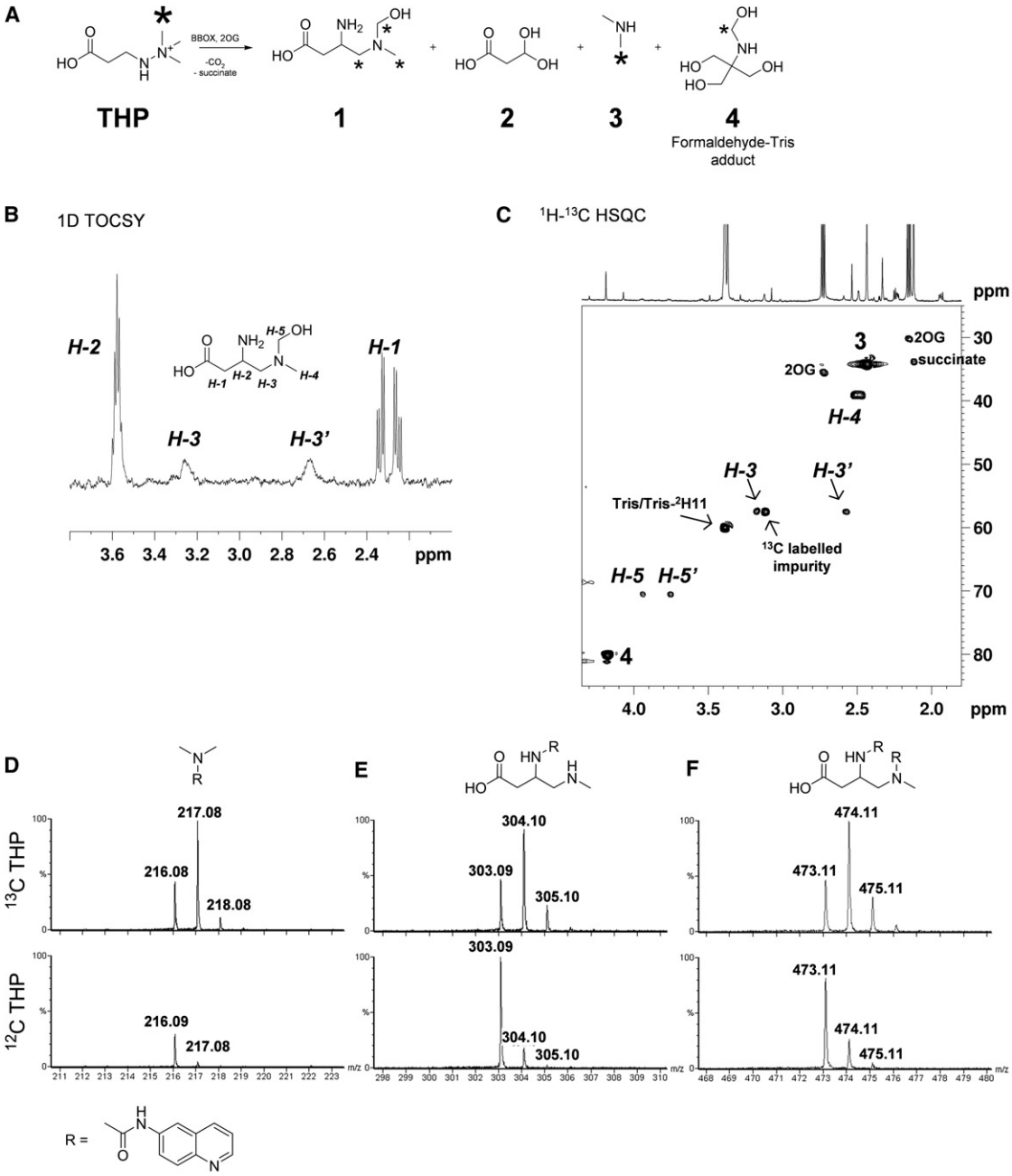

Figure 4. THP Reacts with BBOX in an Unprecedented Reaction

(A) Four products are observed in the THP reaction.

(B) 1D TOCSY of **1** confirming the four carbon chain. Selective excitation is applied on *H-2* at 3.58 ppm.

(C) 2D HSQC showing the reaction of THP labeled with ^{13}C on one of its methyl groups with BBOX. The ^{13}C label (*) is transferred to **3** ($^{1}J_{CH}$ = 143 Hz) and **4** ($^{1}J_{CH}$ = 160 Hz), and C-3, C-4 ($^{1}J_{CH}$ = 141 Hz) and C-5 of **1**, therefore confirming the formation of a new C-C bond. 2OG, succinate and Tris/Tris-$^{2}H_{11}$ are observed at natural abundance ^{13}C levels. The ^{13}C-labeled impurity was present in the starting material. **1** is shown as its formaldehyde adduct, on the basis of further NMR analyses (Figure S4ii).

Reaction of BBOX with unlabeled THP (bottom row) or ^{13}C-labeled THP (top row) with 6-*N*-aminoquinolyl-*N*-hydroxysuccinimidyl carbamate enabled the identification of the carbamoyl derivatives of: (D) dimethylamine **3** (m/z = ^{12}C 216.1 and ^{13}C 217.1);

(E) a singly derivatized product from **1** (m/z = ^{12}C 303.1 and ^{13}C 304.1), and (F) a doubly derivatized product derived from **1** (m/z = ^{12}C 473.1 and ^{13}C 474.1). In the assay containing ^{13}C-labeled THP, the isotope peak abundance is in accordance with the expected product ratio based on the proposed mechanism (Figure 5). In the assay containing unlabeled THP, the isotope peak abundance reflects natural abundance levels.

See also Table S1 and Figure S4 BBOX product characterization.

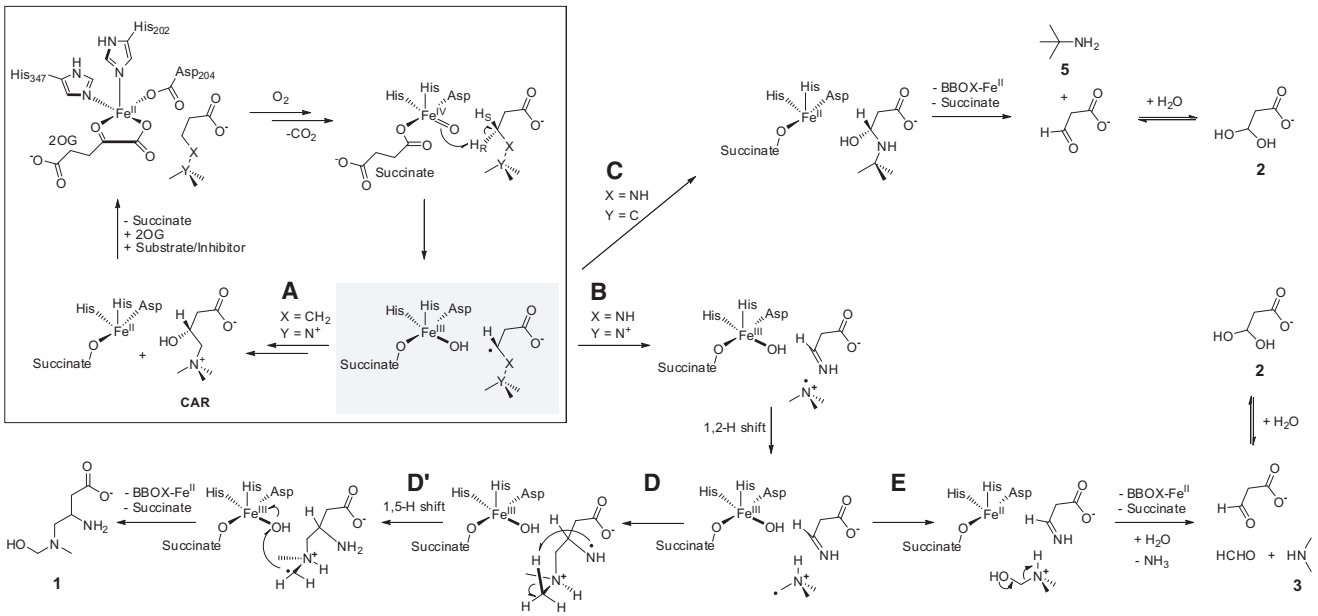

Figure 5. Mechanism for BBOX Catalysis

Proposed mechanisms for the reaction of γBB (route in A), THP (route in B), and 3-*tert*-butylamino propionic acid (route in C) with BBOX. See also Figure S5 for the Stevens rearrangement mechanism.

rebound hydroxylation to give the rearranged product **1**. Analysis of the BBOX-THP structure is consistent with the proposed mechanism; in particular one of the N-methyl groups of THP is close to the metal (N-methyl C to Zn: 5.2 Å cf. C-3 of THP to Zn: 4.7 Å) (Me*) (Figure S3ii). The unprecedented nature of the BBOX-catalyzed THP rearrangement further expands the scope of reactions catalyzed by 2OG oxygenases and may inspire the design of improved inhibitors for BBOX and other 2OG oxygenases.

SIGNIFICANCE

Carnitine plays an essential role in the metabolism of many organisms by enabling transport of fatty acids into mitochondria. Although produced endogenously in humans, carnitine is also used in food supplements. The starting material for carnitine biosynthesis is N^{ε}-trimethyllysine, which is produced from the degradation of posttranslationally modified proteins. Crystallographic studies of γ-butyrobetaine hydroxylase (BBOX), which catalyzes the final step in carnitine biosynthesis, reveal how it binds to its substrates and support prior kinetic analysis. They also highlight structural links between BBOX and histone demethylases, which also employ a ferrous iron cofactor and 2OG and O_2 co-substrates. The structural studies will be useful in the design of improved BBOX inhibitors and more selective inhibitors of other human 2OG oxygenases, which are currently being targeted for therapeutic intervention. Structural and mechanistic studies of the mode of BBOX inhibition by the clinically used compound THP reveal a rearrangement reaction for which there is no direct analog in synthetic chemistry.

EXPERIMENTAL PROCEDURES

Protein Production

The full-length gene of human *BBOX1* was cloned into the pFastBac vector (Invitrogen) containing a tobacco etch virus (TEV) cleavable N-terminal hexahistidine tag. Recombinant baculovirus was produced following the manufacturer's instructions (Invitrogen). High Five cells (Invitrogen) were grown as a suspension in Sf-900 II medium supplemented with 1% fetal calf serum (FCS) at 27°C. Cells were infected at a density of 2 × 10^6/ml with recombinant baculovirus (1 ml of virus stock/1 liter of cell culture). Seventy-two hours after infection, the cultures were collected and centrifuged (30 min, 2000 rpm, 4°C). The cell pellet was resuspended in cold phosphate-buffered saline (PBS) and centrifuged as before. The pellet from 1 liter of culture was then resuspended in 25 ml lysis buffer (50 mM HEPES [pH 7.5], 500 mM NaCl, 5 mM imidazole, 5% glycerol 0.1% v/v Igepal CA 630 (octylphenoxy)polyethoxyethanol, EDTA-free Complete Protease Inhibitor kit (Roche), benzonase (2.5 U/1 ml of a lysate), and 1 mM TCEP *tris*(2-carboxyethyl)phosphine). Cells were lysed using a Dounce homogenizer, followed by centrifugation (45 min, 20, 000 rpm, 4°C). The supernatant was incubated with the Ni-NTA resin for 1 hr with gentle mixing at 4°C. The resultant resin suspension was loaded on a gravity column, and after washing with 50 volumes of resin with washing buffer containing 50 mM HEPES (pH 7.5), 500 mM NaCl, 5% glycerol, and 10 mM imidazole, protein was eluted with 50 mM HEPES (pH 7.5), 500 mM NaCl, and 5% glycerol containing 250 mM imidazole buffer. Fractions were analyzed by SDS-PAGE. Fractions containing BBOX were combined. After EDTA treatment (final concentration 1 mM) at 4°C to remove excess Ni^{2+}, the protein sample was applied to a Superdex 200 16/60 gel-filtration column, which had been equilibrated in 50 mM HEPES (pH 7.5), 500 mM NaCl, 5% glycerol, and 1 mM TCEP. Fractions containing BBOX were combined, and the N-terminal tag was removed by treatment with TEV protease (o/n digestion at 4°C). The protein was diluted with 25 mM Tris buffer (pH 8.0) to 50 mM NaCl. The cleaved BBOX1, residual uncleaved BBOX1, and TEV protease were separated on HiTrap Q Sepharose column, using NaCl gradient (50–250 mM). Fractions containing purified BBOX were combined and concentrated using 30 kDa MWCO concentrator (Amicon).

Crystallization

Crystallization was performed in crystallization plates (SWISSCI, Zug, Switzerland) in a 96-well (three subwell) format. A Mosquito® (TTP Labtech)

Table 1. Data Collection and Refinement Statistics

	BBOX1: γBB (Hg SAD)	BBOX:THP
Data Collection		
Space group	*H*32	*H*32
Cell dimensions		
a, b, c (Å)	107.39, 107.39, 204.92	107.37, 107.37, 205.05
α, β, γ (°)	90, 90, 120	90, 90, 120
Resolution (Å) (outer shell)	28.98–1.78 (1.88–1.78)	20–1.82 (1.92–1.82)
No. of molecules/ASU	1	1
No. of unique reflections	43,809	40,755
Completeness (%)	100.0 (100.0)	99.4 (96.2)
Redundancy	11.0 (10.7)	5.5 (5.3)
R_{sym} [a]	0.140 (0.865)	0.083 (0.452)
Mean I/σ (I)	12.3 (2.9)	12.3 (3.3)
Wilson B value (Å^2)	18.6	21.0
Phasing		
Resolution (Å)	28.82–1.78	
R_{cullis} [b]	0.846 (iso)/ 0.592 (ano)	
Phasing power	0.909 (iso)/ 2.036 (ano)	
Figure of merit		
Centric	0.10831	
Acentric	0.09341	
After density modification	0.865	
Refinement		
R_{factor} [c]	0.14717	0.14671
R_{free} [d]	0.17633	0.18257
Rmsd		
Bond length (Å)	0.016	0.019
Bond angle (°)	1.554	1.600
No. of atoms		
Protein	3192	3149
Ligand/ion	42	62
Water	437	413
<B_{factor}> (Å^2)		
Protein	26.19	30.70
Ligand/ion	26.23	24.83
Water	28.79	31.46

Numbers in parentheses refer to the highest resolution shell.
[a] R_{sym} is the unweighted R value on I between symmetry mates.
[b] $R_{cullis} = \sum_{hkl} ||FPH \pm FP| - FH(calc)| / \sum_{hkl} |FPH \pm FP|$.
[c] $R_{factor} = \sum_{hkl} ||Fobs| - k|Fcalc|| / \sum_{hkl} |Fobs|$ for the working set of reflections.
[d] R_{free} is the R value for 5% of the reflections excluded from refinement.

nanoliter liquid handler was used to set up crystallization plates for coarse screening and optimization of hits. The protein (20 mg/ml) was supplemented with *N*-oxalylglycine (8 mM) and γBB or THP (4 mM) prior to crystallization. Crystals were grown at 20°C using the sitting drop vapor diffusion method by mixing 100 nl of the protein solution and 50 nl of a precipitant solution (0.2 M ammonium citrate [pH 7.0], 20% PEG 3350, 6% hexane-1,6-diamine, and 10 mM ZnSO4). Crystals were flash cooled in liquid nitrogen using 25% glycerol in mother liquor as a cryoprotectant.

A mercury derivative was prepared by incubating BBOX:γBB crystals for 60 min in a reservoir solution containing 10 mM thiomersal. Crystals were then transferred for 1 min to a reservoir solution without mercury but supplemented with 25% ethylene glycol, and crystals were immediately flash frozen in liquid nitrogen.

Data Collection and Processing

Data for BBOX crystals in complex with γBB and THP were collected at DIAMOND beamline I02. Single-wavelength anomalous dispersion (SAD) data using 1.0084 Å wavelength X-rays were collected at DIAMOND beamline IO3 on a crystal derivatized with mercury. Data were integrated using XDS and subsequently scaled using SCALA, whereas data of the mercury derivative were integrated and scaled with the HKL2000 package (Table 1).

Crystallographic Phasing and Refinement

SHELXD was used to locate two mercury positions. Heavy atom positions were refined, and initial phases were calculated with SHARP by using a SIRAS method with the data of BBOX serving as the native data set. The final electron density map after phase extension and solvent flattening with SOLOMON was of excellent quality, and automated model building with ARP/wARP resulted in a 95% complete model. Refinement of both structures used REFMAC. After several rounds of manual rebuilding in COOT and subsequent cycles of refinement, the models converged to a final R_{factor}/R_{free} of 14.7%/17.6% and 14.6%/18.3% for BBOX:γBB and BBOX:THP, respectively (Table 1).

Assays

NMR Assays

NMR experiments were conducted at 700 MHz using a Bruker Avance III spectrometer equipped with an inverse TCI cryoprobe optimized for ^{1}H observation and 3 mm diameter Bruker MATCH micro tubes (Hilgenberg) containing 160 μl final sample volume. Solutions were buffered using Tris or Tris-$^2H_{11}$ (pH 7.5) dissolved 100% D_2O or 95% H_2O/5% D_2O. Pulse tip-angle calibration using the single-pulse nutation method was undertaken for each condition using a blank assay sample . Reaction products are identified and assigned by a combination of multiplicity edited HSQC, HMBC, 1D-TOCSY, and COSY where applicable.

Kinetic Analyses

Standard kinetic assays were conducted at 298 K in solutions containing 12.5 nM BBOX, 50 μM Fe(II), 50 μM substrate, 1.5 mM 2OG, 5 mM ascorbate, 50 mM Tris-$^2H_{11}$ (pH 7.5), and 80 mM KCl. Reactions were started by the addition of BBOX. Kinetic time courses were followed by using standard ^{1}H acquisition (ten transients with a relaxation delay of 1.2 s). The total time lapse between addition of the enzyme and the end of the first acquisition was 4 min. Time courses were followed for at least 15 min, and each measurement was repeated at least three times.

Inhibition Assays

Inhibition assays were conducted at 298 K in solutions containing 12.5 nM BBOX, 50 μM Fe(II), 50 μM γBB, 1.5 mM 2OG, 5 mM ascorbate, 50 mM Tris-$^2H_{11}$ (pH 7.5), 80 mM KCl, and varying concentrations of inhibitor. Reactions were initiated by BBOX addition. The extent of turnover of γBB to give CAR was measured 3 min 45 s after mixing by using standard ^{1}H acquisition (ten transients with a relaxation delay of 1.2 s). Response curves were fitted using OriginPro 8.0 (OriginLab, Northampton, MA, USA). Each measurement was repeated at least three times.

MS Assays

MS experiments were conducted using a Waters LCT Premier XE (Waters, Milford, MA, USA) and/or Bruker MicrOTOF. Assay conditions were as for the NMR work, except that the solution was buffered in 100% H_2O Tris-$^2H_{11}$ (pH 7.5); quenching was by addition of 80% MeCN.

Derivatization Assay

The rearrangement product obtained by reacting THP and ^{13}C-labeled THP in the presence of BBOX was identified using the following procedure. Assay conditions were as for the NMR work, and experiments were quenched by addition of 10% MeCN. The samples were freeze-dried, and the mixture was reacted in borate buffer with 6-*N*-aminoquinolyl-*N*-hydroxysuccinimidyl carbamate according to the supplier's instructions (Waters, Milford, MA, USA), followed by MS analysis of the resulting mixture using a Waters LCT Premier XE.

ACCESSION NUMBERS

The structures have been deposited in the RCSB Protein Data Bank as ID 3MS5 and 3O2G.

SUPPLEMENTAL INFORMATION

Supplemental Information includes Supplemental Experimental Procedures, five figures, and one table and can be found with this article online at doi:10.1016/j.chembiol.2010.09.016.

ACKNOWLEDGMENTS

We thank the Engineering and Physical Sciences Research Council, Berrow Foundation, Biotechnology and Biological Sciences Research Council, and the Wellcome Trust for support. The Oxford Structural Genomics Consortium is a registered UK charity (number 1097737) that receives funds from the Canadian Institutes for Health Research, the Canadian Foundation for Innovation, Genome Canada through the Ontario Genomics Institute, GlaxoSmithKline, Karolinska Institutet, the Knut and Alice Wallenberg Foundation, the Ontario Innovation Trust, the Ontario Ministry for Research and Innovation, Merck & Co., Inc., the Novartis Research Foundation, the Swedish Foundation for Strategic Research, and the Wellcome Trust. The work was also supported by the NIHR Biomedical Research Unit. We thank the staff at Diamond Light Source for assistance, support, and access to the beamline. We thank Dr. James McCullagh, Colin Sparrow, and Nikita Loik for their support and advice on this project.

Received: August 11, 2010
Revised: September 9, 2010
Accepted: September 13, 2010
Published: December 21, 2010

REFERENCES

Brass, E.P., Hoppel, C.L., and Hiatt, W.R. (1994). Effect of intravenous L-carnitine on carnitine homeostasis and fuel metabolism during exercise in humans. Clin. Pharmacol. Ther. *55*, 681–692.

Bremer, J. (1983). Carnitine—metabolism and functions. Physiol. Rev. *63*, 1420–1480.

Clifton, I.J., McDonough, M.A., Ehrismann, D., Kershaw, N.J., Granatino, N., and Schofield, C.J. (2006). Structural studies on 2-oxoglutarate oxygenases and related double-stranded β-helix fold proteins. J. Inorg. Biochem. *100*, 644–669.

Curran, D.P., Kim, D., Liu, H.T., and Shen, W. (1988). Translocation of radical sites by intramolecular 1,5-hydrogen atom transfer. J. Am. Chem. Soc. *110*, 5900–5902.

Dambrova, M., Liepinsh, E., and Kalvinsh, I. (2002). Mildronate: cardioprotective action through carnitine-lowering effect. Trends Cardiovasc. Med. *12*, 275–279.

Englard, S., Blanchard, J.S., and Midelfort, C.F. (1985). γ-Butyrobetaine hydroxylase: stereochemical course of the hydroxylation reaction. Biochemistry *24*, 1110–1116.

Furusawa, H., Sato, Y., Tanaka, Y., Inai, Y., Amano, A., Iwama, M., Kondo, Y., Handa, S., Murata, A., Nishikimi, M., et al. (2008). Vitamin C is not essential for carnitine biosynthesis in vivo: verification in vitamin C-depleted senescence marker protein-30/gluconolactonase knockout mice. Biol. Pharm. Bull. *31*, 1673–1679.

Galland, S., Le Borgne, F., Guyonnet, D., Clouet, P., and Demarquoy, J. (1998). Purification and characterization of the rat liver gamma-butyrobetaine hydroxylase. Mol. Cell. Biochem. *178*, 163–168.

Hausinger, R.P. (2004). Fe(II)/α-ketoglutarate-dependent hydroxylases and related enzymes. Crit. Rev. Biochem. Mol. Biol. *39*, 21–68.

Hoffart, L.M., Barr, E.W., Guyer, R.B., Bollinger, J.M., and Krebs, C. (2006). Direct spectroscopic detection of a C-H-cleaving high-spin Fe(IV) complex in a prolyl-4-hydroxylase. Proc. Natl. Acad. Sci. USA *103*, 14738–14743.

Holme, E., Lindstedt, S., and Nordin, I. (1982). Uncoupling in the γ-butyrobetaine hydroxylase reaction by D- and L-carnitine. Biochem. Biophys. Res. Commun. *107*, 518–524.

Horton, J.R., Upadhyay, A.K., Qi, H.H., Zhang, X., Shi, Y., and Cheng, X. (2010). Enzymatic and structural insights for substrate specificity of a family of jumonji histone lysine demethylases. Nat. Struct. Mol. Biol. *17*, 38–43.

Huang, Y., Fang, J., Bedford, M.T., Zhang, Y., and Xu, R.M. (2006). Recognition of histone H3 lysine-4 methylation by the double Tudor domain of JMJD2A. Science *312*, 748–751.

Hulse, J.D., Ellis, S.R., and Henderson, L.M. (1978). Carnitine biosynthesis. β-Hydroxylation of trimethyllysine by an α-ketoglutarate-dependent mitochondrial dioxygenase. J. Biol. Chem. *253*, 1654–1659.

Krebs, C., Fujimori, D.G., Walsh, C.T., and Bollinger, J.M. (2007). Non-heme Fe (IV)-oxo intermediates. Acc. Chem. Res. *40*, 484–492.

Krissinel, E., and Henrick, K. (2007). Inference of macromolecular assemblies from crystalline state. J. Mol. Biol. *372*, 774–797.

Lindstedt, G. (1967). Hydroxylation of γ-butyrobetaine to carnitine in rat liver. Biochemistry *6*, 1271–1282.

Lindstedt, G., Lindstedt, S., and Nordin, I. (1977). Purification and properties of γ-butyrobetaine hydroxylase from Pseudomonas sp AK 1. Biochemistry *16*, 2181–2188.

Naidu, G.S.N., Lee, I.Y., Lee, E.G., Kang, G.H., and Park, Y.H. (2000). Microbial and enzymatic production of L-carnitine. Bioprocess Biosyst. Eng. *23*, 627–635.

Ng, S.S., Kavanagh, K.L., McDonough, M.A., Butler, D., Pilka, E.S., Lienard, B.M.R., Bray, J.E., Savitsky, P., Gileadi, O., von Delft, F., et al. (2007). Crystal structures of histone demethylase JMJD2A reveal basis for substrate specificity. Nature *448*, 87–92.

Simkhovich, B.Z., Shutenko, Z.V., Meirena, D.V., Khagi, K.B., Mezapuķe, R.J., Molodchina, T.N., Kalviņs, I.J., and Lukevics, E. (1988). 3-(2,2,2-Trimethylhydrazinium) propionate (THP)—a novel gamma-butyrobetaine hydroxylase inhibitor with cardioprotective properties. Biochem. Pharmacol. *37*, 195–202.

Spaniol, M., Brooks, H., Auer, L., Zimmermann, A., Solioz, M., Stieger, B., and Krähenbühl, S. (2001). Development and characterization of an animal model of carnitine deficiency. Eur. J. Biochem. *268*, 1876–1887.

Stevens, T.S. (1928). Degradation of quaternary ammonium salts. Part I. J. Chem. Soc., 3193–3197.

Tars, K., Rumnieks, J., Zeltins, A., Kazaks, A., Kotelovica, S., Leonciks, A., Saripo, J., Viksna, A., Kuka, J., Leipinsh, E., and Dambrova, M. (2010). Crystal structure of human gamma-butyrobetaine hydroxylase. Biochem. Biophys. Res. Commun. *398*, 634–639.

Vanecko, J.A., Hayley, W., and West, F.G. (2006). Recent advances in the Stevens rearrangement of ammonium ylides. Tetrahedron *62*, 1043–1062.

Vaz, F.M., and Wanders, R.J.A. (2002). Carnitine biosynthesis in mammals. Biochem. J. *361*, 417–429.

Wehbie, R.S., Punekar, N.S., and Lardy, H.A. (1988). Rat liver γ-butyrobetaine hydroxylase catalyzed reaction: influence of potassium, substrates, and substrate analogues on hydroxylation and decarboxylation. Biochemistry *27*, 2222–2228.

Zhang, Z., Ren, J.-S., Harlos, K., McKinnon, C.H., Clifton, I.J., and Schofield, C.J. (2002). Crystal structure of a clavaminate synthase-Fe(II)-2-oxoglutarate-substrate-NO complex: evidence for metal centered rearrangements. FEBS Lett. *517*, 7–12.

